Journal of Microscopy

Journal of Microscopy, Vol. 273, Issue 3 2019, pp. 169–177 doi: 10.1111/jmi.12771
Received 11 June 2018; accepted 13 November 2018

The 3D imaging of mesenchymal stem cells on porous scaffolds using high-contrasted x-ray computed nanotomography

L. VOJTOVÁ*, T. ZIKMUND*, V. PAVLIŇÁKOVÁ*, J. ŠALPLACHTA*, D. KALASOVÁ*, E. PROSECKÁ†, J. BRTNÍKOVÁ*, J. ŽÍDEK*, D. PAVLIŇÁK‡ & J. KAISER*

**CEITEC, Brno University of Technology, Brno, Czech Republic*

†Institute of Experimental Medicine ASCR v.v.i., Prague, Czech Republic

‡CEPLANT, Department of Physical Electronics, Masaryk University, Brno, Czech Republic

Key words. Biopolymeric scaffold, mesenchymal stem cells, SEM/EDX, tissue engineering, X-ray computed nanotomography.

Summary

This study presents an X-ray computed nanotomography (nano-CT) based, high-resolution imaging technique. Thanks to a voxel resolution of 540 nm, this novel technique is suitable for observing the 3D morphology of soft biopolymeric scaffolds seeded with stem cells. A sample of highly porous collagen scaffold seeded with contrasted mesenchymal stem cells (MSC) was investigated by using lab-based nano-CT. The whole volume of the sample was analysed without its destruction. To evaluate the potential of nano-CT, a comparison measurement was done using a standard microscopy technique. Scanning electron microscopy (SEM) combined with energy dispersive X-ray analysis (EDX) established an extension and local accumulation of the contrasting agent – heavy metallic osmium tetroxide. The presented imaging technique is novel as it will help to understand better the behaviour of cells while interacting with three-dimensional biomaterials. This is crucial for both experimental and clinical tissue engineering applications in order to limit the risk of uncontrolled cell growth, and potentially tumour formation.

Introduction

In recent years, some resorbable porous cell and drug carriers, generally named scaffolds, which are based on biopolymer composites, have been developed. These scaffolds are used with successful preclinical results for a treatment of bone and cartilage by applying tissue engineering methods (Prosecká *et al.*, 2011; Prosecká *et al.*, 2015). It has been confirmed that namely collagen-based 3D porous scaffolds represent an ideal matrix for the deposition of cells such as mesenchymal stem cells (MSC) or already differentiated chondrocytes. Even though the scaffolds were implanted into a damaged tissue, cell growth continued as in common living tissue (Van der Rest & Garrone, 1991; Jančář *et al.*, 2009; Nečas *et al.*, 2010).

The morphology of porous biopolymer scaffolds is usually observed using scanning electron microscopy (SEM); however, SEM micrographs enable to visualise only two-dimensional (2D) images of fractured surfaces. The real three-dimensional (3D) shape and connectivity of pores cannot be imaged or quantified without using stereology. Despite the steady progress in the field of electron microscopy, polymeric and ceramic scaffolds have to be coated with an electric conductive layer, which make the technique destructive especially if high beam intensity is needed. However, for both *in vitro* and *in vivo* tests or for clinical trials it is necessary to know the exact structure of pore network before and also after the implantation within the responses of living cells. Therefore, a nondestructive characterisation technique is required for a quantification. Moreover, 3D imaging and quantification of tissue regeneration using degradable polymer scaffolds is a useful and desirable part of every bio-technological research.

The most common 3D imaging method used for examining cells proliferated in the artificially created scaffolds is confocal reflection fluorescence microscopy (Moore *et al.*, 2004; Oliveira *et al.*, 2007; Oliveira *et al.*, 2010). However, a limited depth resolution of about 300 μm, cell's invasive staining and a requirement of substrate transparency prevent from using this method for larger opaque tissue engineering constructs. Other common methods for measuring the cell presence include the colorimetric and fluorometric assays for enzymes (dehydrogenase), proteins (BCA), RNA or DNA (PicoGreen assay). The main disadvantage of these assays is the missing information about the cell distribution in the whole volume of the sample The 3D real-time observation of live cells' properties in scaffold's microenvironments, such as morphology, motility and migration using multimodal holographic microscopy

Correspondence to: T. Zikmund, CEITEC, Brno University of Technology, Purkyňova 656/123, 612 00 Brno, Czech Republic. Tel: +420 541 142 846; email: tomas.zikmund@ceitec.vutbr.cz

(Q-Phase microscope), enable a quantitative measurement of cell mass movement (Collaková *et al.*, 2015, Kollarova *et al.*, 2015). The 3D real time observation methods are less known but very advanced. There is no need of the cell contrasting; however, the scaffold has to be transparent. Moreover, the method does not provide any information about the scaffolds' structure.

Due to the recent progress in the 3D imaging methods and image analysis strategies, X-ray high-resolution micro focus computed tomography (micro-CT) has been commonly applied as a nondestructive technique for visualising the scaffolds' interior by providing quantitative information of scaffolds' 3D morphology as well as of bone ingrowth after in vivo scaffold implantation (Yang *et al.*, 2008; Komlev *et al.*, 2009; Cedola *et al.*, 2014; Sun *et al.*, 2014). CT has been used to scan hard tissues (Taboas *et al.*, 2003; Hofmann *et al.*, 2007; Mather *et al.*, 2008). As for soft tissues and tissue replacements, their scanning of soft tissues and tissue replacements is more complex, due to their low linear attenuation coefficient (Momose *et al.*, 1996). In comparison with hard tissue objects, the weak contrast of soft biological materials in CT has contributed to the phase contrast imaging technique development (Bech *et al.*, 2009; Kalasová *et al.*, 2016). Synchrotron radiation-based CT systems provide better phase contrast because the synchrotron source generates an X-ray with high spatial coherence and high flux, which has been used for an investigation of cells in the extracellular matrix (Albertini *et al.*, 2009; Giuliani *et al.*, 2014). Gros *et al.* (2005) compared various types of X-ray microscopes for synchrotron radiation which could be used for an imaging of, for example, yeast or *Escherichia coli*. Schneider *et al.* (2002) focused on the visualisation of immune-gold labelled *Drosophila melanogaster* cells using cooling capillary for the sample. A study published by Larabell & Gross (2004) describes 3D reconstructions of *Saccharomyces cerevisiae* using photon energies just below the oxygen edge (i.e. 517 eV). Synchrotron-based nano-CT has been used for a calcium distribution in coccolithophores (Sun *et al.*, 2014). The synchrotron imaging quality is exceptional; however, the method's availability is restricted. Along with the recent development of X-ray micro and nanofocus tubes and X-ray detectors, tomographic imaging of biomaterials becomes available also with laboratory sources. Lab-based CT enables an observation of structures with a voxel resolution from micron (micro-CT) to submicron (nano-CT). The phase contrast effect might be observed also with laboratory nano-CT devices (Kaiser *et al.*, 2011). Khoury *et al.* (2015) compared two tomographic lab-based systems, micro-CT and nano-CT. Among others, they showed that these systems enable measurements with various resolutions implemented on object size in the range coming from mouse organ down to cellular level. Nano-CT technique was also utilised for the visualisation of cell-free soft collagen-based scaffolds (Žídek *et al.*, 2016) or hard titanium alloy scaffolds with periosteum-derived cells (Papantoniou *et al.*, 2014).

Unfortunately, the aforementioned studies did not provide a simultaneous visualisation of both soft scaffold environment and MSC due to their small size in the range from 10 to 35 μm (Ge *et al.*, 2014; Kampschulte *et al.*, 2016). Moreover, a 3D visualisation of MSC seeded on collagen-based scaffolds done by using CT imaging methods depends on choosing the most suitable contrast agent. The reason is that some of the agents, such as collagen and fibrin, are specifically bonded to connective (Balint *et al.*, 2000; Metscher, 2009; Herzog *et al.*, 2013; Tesařová *et al.*, 2016).

In this study, we used a high-resolution, high-contrast X-ray microscope Rigaku Nano3DX with an ability to deliver 3D nano-CT images of relatively large samples at a high voxel resolution down to 270 nm. The Nano3DX enables to change the target, meaning the X-ray wavelength, and sample-detector distance. Thanks to this variability it is possible to some extent to make an experimental setup suitable for phase contrast imaging. However, the following conditions must be fulfilled: avoiding geometrical unsharpness due to the finite focal spot size of the X-ray tube (Lubberts & Rossmann, 1967), imaging in an edge-detection regime (Baruchel, 2000), maintaining a sufficient degree of X-ray tube coherency (Wu & Liu, 2007). Phase contrast imaging is a CT imaging method suitable for light biological materials which do not have a sufficient absorption contrast. However, in this work osmium tetroxide X-ray opaque staining (Hildore *et al.*, 2007) has to be used in order to visualise MSCs seeded on porous collagen scaffold. Experimental conditions were set to meet the conditions' requirements necessary for phase contrast imaging. The phase contrast effects were utilised for edge-enhancement. This novel 3D imaging method helps to understand the biomaterial/cell interactions in the whole volume, which is applicable in cell biology, tissue engineering and modern medicine.

Results

Prior to the nano-CT visualisation using X-ray microscope, the SEM equipped with an energy dispersive X-ray (EDX) for the elemental analysis was used to characterise MSCs proliferated on collagen scaffolds (Fig. 1A). To enhance the contrast and MSCs distinction from the collagen matrix in the nano-CT scan, the cells seeded on collagen scaffold were fixed at day 21. Consequently, their continuous proliferation throughout the scaffold followed by staining with OsO_4 was seen. Elemental distribution of osmium confirmed our first hypothesis that osmium is spread not only on the MSCs surface but also partly on the entire scaffold surface as it can be seen in Figure 1. However, the increased osmium concentration was predominantly detected on cells' surface (Figs. 1B and C, respectively). Different concentration of OsO_4 (0.1, 0.5 and 1.0 wt %) led to different absorbing properties of MSCs and scaffolds in nano-CT. In this paper we present the optimal OsO_4 concentration equal to 1 wt %.

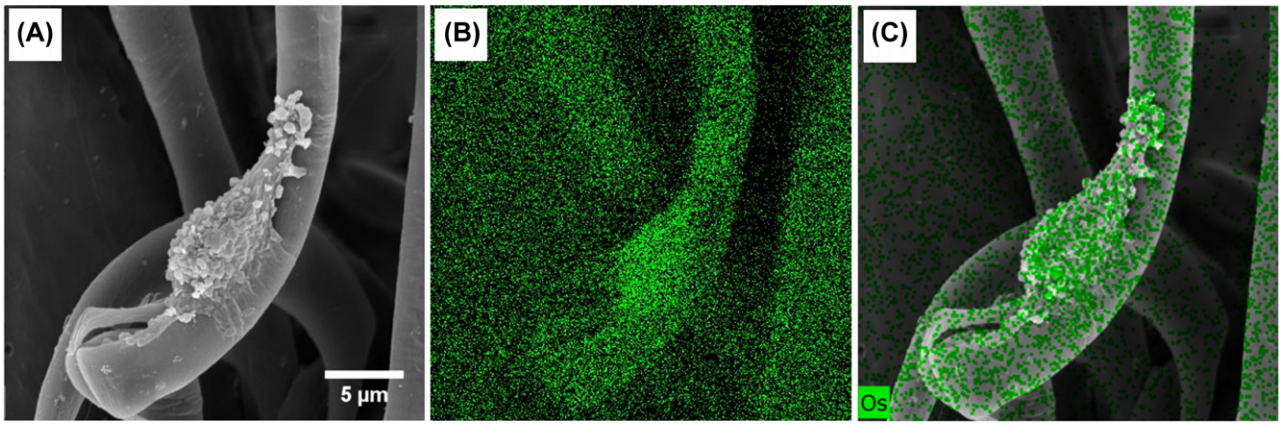

Fig. 1. (A) 2D SEM image of collagen fibre in scaffold with adhered MSC, (B) EDX mapping analysis of osmium distribution in the surface of the specimen, (C) EDX mapping analysis of osmium distribution in the surface of the specimen merged with SEM image as a substrate.

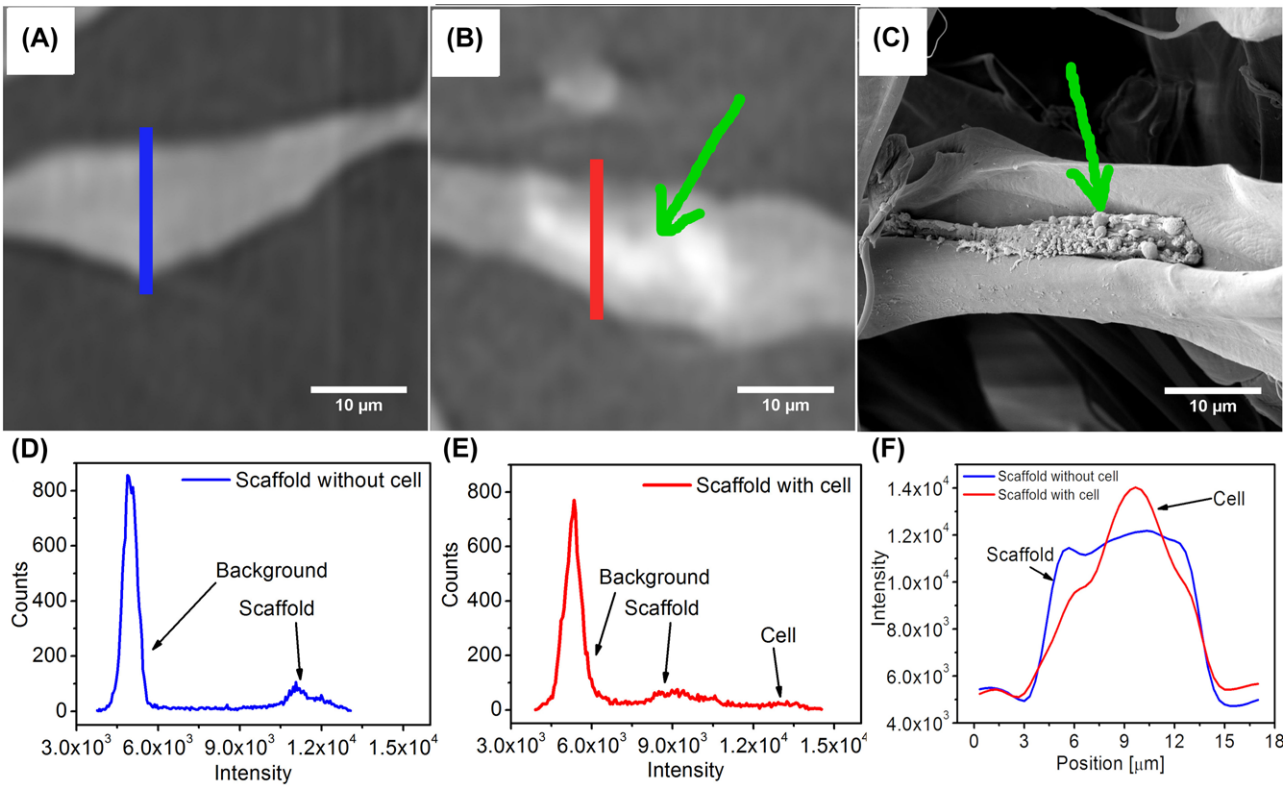

Fig. 2. Collagen scaffold seeded with MSCs integrated inside of the collagen scaffold structure: (A) selected nano-CT slice of collagen fibre without cell presence with labelled blue area for line profile analysis – intersection from CT slice with scaffold structure without cells, (B) a slice from nano-CT including MSCs (light area) inside the scaffold structure with labelled red area for line profile analysis – intersection from CT slice with scaffold structure with cells, (C) an appropriate image from scanning electron microscopy. Green arrow shows the cell, CT images were magnified according to SEM scale. (D) Histogram of grey levels for Figure 2(A), (E) a histogram of grey levels for Figure 2(B) and (F) result of line profile analysis.

Thanks to the increased osmium concentration on the MSC surface, we detected higherintensities of the MSCs compared to collagen scaffold in nano-CT data (Figs. 2A, B). As it is obvious, reference sample was homogeneously visualised by grayscale through its volume (Fig. 2A). The sample showed a contour of collagen fibril. In comparison with the reference sample, the tomographic slice of the seeded scaffold included light areas inside the scaffold structure (Fig. 2B). The brighter area (green arrow) represents a cell separated from the collagen scaffold. These areas were caused by an increased OsO_4 concentration

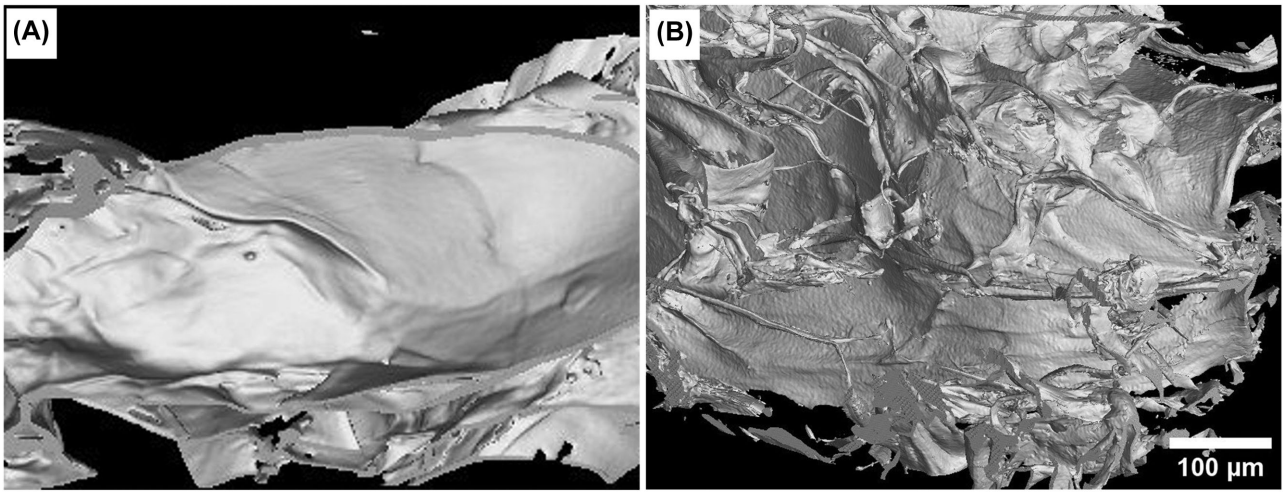

Fig. 3. The comparison of the pure collagen scaffold without MSCs (A) and the collagen scaffold seeded with MSCs at the same magnification (B).

in MSCs. Both SEM and EDX confirmed that the MSC adherent on the fibre inside the collagen scaffold (see supplementary material S1) corresponded with the light area of tomographic slice. A cell from the same sample was visualised by using scanning electron microscopy with a fine resolution (Fig. 2C). The shape and size of the cell detected in Figure 2(B) is similar to the cell obtained from SEM. Figures 2(D)–2(F) represent histograms of gray levels and intensity profile to better visualise the OsO_4 presence in cells.

The Figure 2 also compares visualisations of 2D projection of samples scanned by nano-CT and SEM. The quality of SEM visualisation is given by high resolution which cannot be reached by nano-CT. On the other hand, the nano-CT scan contains information about 3D structure of the sample. The reconstruction of object from 3D data enables us to improve the visualisation from Figure 2(B) (presented below).

The advantage of SEM is a possibility to visualise the cell structure details. Contrary to this, at nano-CT visualisation results in the cell shape as well as the volume information of cell morphology and the cell distribution within the scaffold. This is important for the investigation of cell growth and proliferation at different time intervals or changes in the scaffold morphology after certain time exposed to the cells. An accurate 3D image of biopolymeric scaffold seeded with MSCs can be reached by a volume reconstruction of nano-CT data (Fig. 3).

In order to confirm the correct distinction of MSCs from the collagen scaffold, we compared the 3D visualisation of the pure collagen cell-free scaffold (Fig. 3A) with the 3D visualisation of the scaffold seeded with MSCs (Fig. 3B). The nano-CT image of pure collagen scaffold exhibited smooth surface without any visible clusters. On the contrary, the surface of the scaffold seeded with the MSCs exhibited uneven morphology consisting of cell arrangements with an average size of around 20 μm.

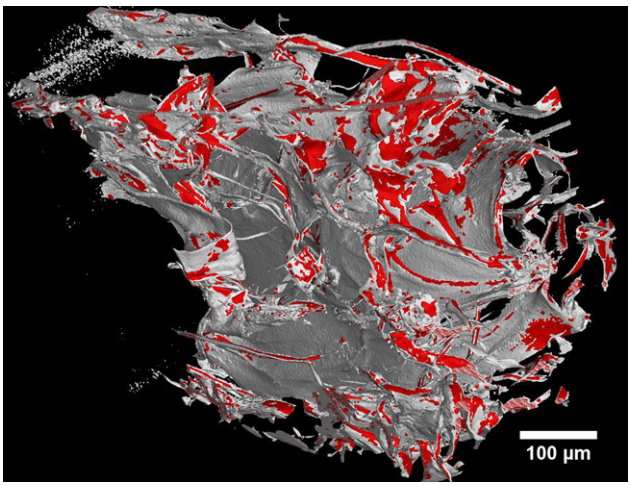

Fig. 4. 3D rendering of MSCs (red colour) proliferated on scaffold surface (grey area). Cells are segmented by simple thresholding method and cover approximately 60% of the visualised object (calculated without air volume).

Based on the previous results showed in Figure 2(B), high intensities of the visualisation in the CT data representing cells were coloured red. The resulting 3D visualisation of the scaffold seeded with MSCs is given in Figure 4 where cells can be recognised more accurately than in the case of 2D slice in Figure 2(B). Therefore, the distribution of cells both within the scaffold volume and on its surface is clearly visible. Based on the 3D rendering it is possible to make the decision whether cells are homogeneously dispersed throughout the scaffold proving their migration and proliferation abilities on a 3D biomaterial substrate.

A more detailed 3D image of the scaffold after the volume rendering exhibited a good adhesion of MSCs to the scaffold surface (Fig. 5). The Figure 5(B) represents the zoomed

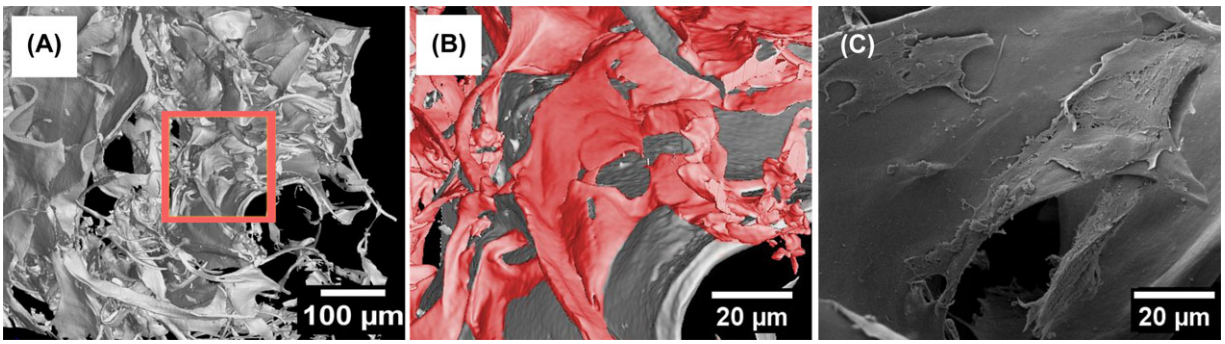

Fig. 5. 3D visualisation of MSCs seeded on the collagen porous scaffold 3D rendering of nano-CT data, (B) detail on the red labelled area from the (A). Cells are manually visualised by red colour. (C) SEM visualisation of MSCs on the collagen scaffold.

rectangle area from Figure 5(A). For a better representation, MSCs were highlighted in red colour (Fig. 5B). Similar MSC size and shape adhering to the scaffold surface were also established by SEM (Fig. 5C).

Discussion

Nowadays, a simultaneous imaging of 3D substrate structure together with incorporated cells is a great challenge in the field of tissue engineering and cell biology. As we previously proved (Žídek *et al.*, 2016), biopolymeric scaffolds could be visualised by a nondestructive 3D nanofocus X-ray CT. However, by this method, we were not able to visualise both biopolymeric scaffold and seeded MSC due to a relatively low voxel resolution of approx. 4 μm. In this paper, we proposed Nano3DX as a novel 3D nano-CT imaging technique to visualise the whole volume of porous collagen scaffold seeded with MSC stained by osmium with a voxel resolution of about 540 nm.

Based on our previous experience from visualising osmium-stained adipose cells on nanofocus CT (unpublished results), we used OsO_4 to stain MSCs in order to increase their contrast on a novel Rigaku Nano3DX nano-CT and to separate them better from the collagen scaffold image. Similarly to Scheller *et al.* (Scheller *et al.*, 2014) who used osmium tetroxide to stain bone marrow adipose tissue for micro-CT visualisation, we reasoned to stain MSCs by osmium to make cells radio dense and therefore visible on nano-CT. OsO_4 was firstly introduced in 1952 (Palade, 1952) to identify the structure and function of cell organelles using the electron microscope. Since OsO_4 is one of the oldest fat stains, unsaturated fat acids like oleic acid (content of phospholipid membranes) are considered to be responsible for the reduction reaction. By an addition of OsO_4 to the double carbon-to-carbon bonds (contained in fats), osmium becomes soluble and forms a black hydrated reduced osmium dioxide compound (Riemersma, 1968). Moreover, osmium is a heavy metal and is radiodense, which shows a higher contrast while using CT. Thanks to this fact it is possible to visualise stained cells. If a polar group as well as double bonds play a part in the reactions, this might explain some electron microscopic findings suggesting that during osmium fixation the deposition of osmium dioxide probably occurs at the polar ends of the organic molecules (Riemersma, 1968). Starborg *et al.* (2013) determined collagen fibril size and its self-assembly by TEM 3D images from embryonic tendon prepared by the reduced osmium staining protocol. 3D images have a sufficient contrast to identify individual collagen fibrils and to obtain quantitative information about the cell number, cell shape, cell-cell interactions and collagen fibril number. The contrast is also sufficient to identify collagen fibrils in cell surface fibripositors.

However, the MSCs seeded the collagen scaffold were difficult to identify because the thickness of flat cells is supposed to be low, depending on the cell adhesion on scaffold, and because the size of a cell is approx. between 10 and 30 μm. Moreover, well-adhered cells appeared to be well attached to the scaffold surface. We distinguished the cells from the collagen matrix based on following criteria. The first criterion was a high osmium concentration inside the cells because OsO_4 binds better to the cell membrane than to the collagen scaffold during the staining process (Bahr, 1954; Hayes *et al.*, 1963). Moreover, our collagen scaffold is chemically cross-linked via polar end-groups (−COOH and $-NH_2$) resulting in nonpolar amide bond (−CONH) thus limiting active sites for OsO_4 binding. Obtained results were confirmed by the elemental analysis and tomographic data. From the tomographic slices and 3D rendering, it was evident that cells were well distributed both on the surface and within the scaffold.

The segmentation of scaffold and cells from the background of CT data is sensitive to the selection of optimal threshold value, which make the quantitative analysis still challenging. The application of the phase retrieval algorithm and denoising filter was crucial improvement leading to achieve a high CT data quality. Moreover, as mentioned above, cells exhibited a higher intensity thanks to the higher concentration of osmium in comparison to pure collagen scaffold (Fig. 2). Other criteria for the segmentation of cells were their size and shape. As it has been revealed by both tomographic data and 3D rendering, the MSCs appeared elongated with the average size of around

20 μm that is in a good acceptance with the study reported by Ge *et al.* (2014).

The presented study demonstrated that the nano-CT is a suitable imaging method for observing cells seeded on scaffold through its entire volume. The 3D nano-CT imaging pictures also enable to separate cells from the scaffold which help to understand better following: the methods of seeding 3D porous scaffolds by cells; the behaviour of cells within the scaffold (their adhesion, migration, proliferation and differentiation at different time intervals); changes in the scaffold morphology after certain time exposed to the cells. These issues are essential in the cell biology and modern tissue engineering concept allowing regeneration of both soft and hard tissue (e.g. skin, cartilage or bone) as well as organs (heart, kidney, liver, lung etc.).

Experimental procedures

Materials

For the scaffold preparation: certified bovine collagen type I was obtained in a freeze-dried form from VUP medical, Ltd. (Czech Republic). *N*-(3-Dimethylaminopropyl)-*N*′-ethylcarbodiimide hydrochloride (EDC), *N*-hydroxysuccinimide (NHS) (Sigma Aldrich, Germany) and $Na_2HPO_4{\cdot}12H_2O$ (Sigma Aldrich) were used as received for scaffold' crosslinking. For the cell culture: Dulbecco's phosphate-buffered saline and heparin were obtained from Zentiva (Czech Republic), Gelofusine from B-Braun (Czech Republic), l-glutamine from PAA (Czech Republic), dexamethasone, ascorbic acid-2-phosphate, and glycerol 2-phosphate disodium salt hydrate from Sigma Aldrich. Fetal bovine serum and penicillin/streptomycin were used as the culture medium.

Scaffold preparation

Collagen porous scaffolds were prepared with slight modification according to the method developed by our group (Sloviková *et al.*, 2008). Briefly, a 0.5 wt % collagen aqueous solution was prepared by disintegration at 8000 rpm. The solution was subsequently centrifuged for 5 min at 2879 × g in order to remove air bubbles. Subsequently, a primary freeze-drying process was applied using Martin Christ Epsilon 2–10D lyophilizator at 35°C under 1 mBar for 15 h followed by secondary drying process at 25°C under 0.01 mBar until decreasing Δp up to 10 %. Dry foamed scaffolds were stabilised by treating with EDC/NHS in ethanol solution, washed with $Na_2HPO_4{\cdot}12H_2O$, flushed with distilled water and freeze-dried again. Prepared collagen scaffolds were sterilised using ethylene oxide gas.

Cell seeding

Our previous study (Prosecká *et al.*, 2015) described an isolation of MSCs from rabbits (age 3 months). The autologous cells in the culture medium were trypsinated, and in the second passage were seeded on the scaffolds at a density of 2×10^6 cm^{-2} in a cultivated 24-well plate modified with the culture medium. The plate was centrifuged at 7G for 20 min and cultured at 37°C in a humidified atmosphere with 5% CO_2. MSCs were cultivated on collagen scaffolds for 21 days, fixed and stained. The Ethical Principles and Guidelines for Scientific Experiments on Animals were respected throughout this study. The maintenance and handling of the experimental animals followed EU Council Group Description Directive (2010/63/EU), and the animals were treated in accordance with the principles of Care and Use of Animals.

Staining

Seeded scaffolds were subsequently rinsed with phosphate-buffered saline (PBS) and transferred to a glutaraldehyde solution (Sigma Aldrich) to fix the cells. Consequently, the cells fixed in scaffolds were stained by immersing in a PBS solution of staining agents, specifically OsO_4 (Sigma Aldrich). For the purpose of a nano-CT comparative study, cell-free crosslinked collagen scaffolds were also stained with osmium.

X-ray computed nanotomography

The nano-CT measurement of scaffolds was performed on a RIGAKU Nano3DX device. This machine is equipped with a 3300×2500 pixel^2 X-ray CCD camera and a Cu rotatory target working at an accelerating voltage of 40 kV and a current of 30 mA. An optical head with 20× magnification was chosen to reach the field of view at 0.7×0.9 mm^2. The sample-detector distance was set to 1.5 mm. This is a satisfactory distance for the X-rays to have a sufficient degree of coherence and to exhibit phase contrast. Binning 2 was set due to a low signal. This determined the linear voxel size of the resulting CT data at 0.54 μm. A total of 800 projections were taken with an exposure time of 10 s.

Image data analysis

In order to increase the image quality and data utilisation for the subsequent analysis the acquired tomographic projections were processed by the series of image analysis techniques before applying the filtered back projection based tomographic reconstruction process. The projections were filtered using an optimised block wise nonlocal means (NLM) denoising filter (Coupe *et al.*, 2008) and movement artefacts were reduced using a custom developed movement correction technique based on the phase correlation. This resulted in an increase of SNR (signal-to-noise ratio) from 41 to 89 and from 59 to 72 in tomogram domain (data after tomographic reconstruction). An application of phase retrieval algorithm increased the contrast between cell and scaffold structure (see Supplementary material S2) having a positive effect on the subsequent cell segmentation. Nano3DX

generates sufficiently coherent X-rays to observe the phase contrast effects via edge-enhancement (Kaiser *et al.*, 2011). The phase retrieval algorithm was applied on filtered and corrected projections using an ANKAphase (Weitkamp *et al.*, 2011) plugin for ImageJ (Rasband, 2017), which implements algorithm by Paganin (Paganin *et al.*, 2002). Then the projections were reconstructed with the ASTRA Toolbox (Aarle *et al.*, 2016; Aarle *et al.*, 2015). The final analysis and visualisation of scaffold structures with MSCs based on surface determination and global thresholding was accomplished using VGStudio MAX software (Palenstijn *et al.*, 2011), where the volume reconstruction of nano-CT data was done by applying the isosurface volume rendering method. Global thresholding with use of manual selected threshold was applied to carry out a quantitative analysis of cell volume.

Scanning electron microscopy (SEM) and elemental analysis (EDX)

Scaffold morphology was investigated employing a scanning electron microscope Tescan Mira3 (Tescan, Czech Republic). If not specified otherwise, the secondary electron emission mode at 15 kV acceleration voltages was used for all observations. In order to achieve a better resolution, samples were coated with a 20 nm of gold layer. The surface elemental analysis was determined by Energy Dispersive X-ray Spectroscopy (EDX) (Oxford Instruments) and evaluated by Aztec 2.1a software.

Author contributions

LV, TZ, VP, D K the interpretation of results; VP, LV, TZ writing the manuscript; VP collagen scaffold preparation; EP cell seeding; JB, DP SEM and EDX analysis; DK nano-CT measurement; JŠ, DK, DP, JŽ image analysis; JK supervisor of the project. All authors read and approved the final manuscript.

Acknowledgements

This research was carried out under the project CEITEC 2020 (LQ1601) with financial support from the Ministry of Education, Youth and Sports of the Czech Republic under the National Sustainability Programme II. This research has been also supported by the project CZ.1.05/2.1.00/03.0086 funded by European Regional Development Fund and project LO1411 (NPU I) funded by Ministry of Education, Youth and Sports of Czech Republic as well as support from the Ministry of Health of the Czech Republic under grant number 17–31276A.

References

Albertini, G., Giuliani, A., Komlev V., *et al.* (2009) Organization of extracellular matrix fibers within polyglycolic acid-polylactic acid scaffolds analyzed using X-ray synchrotron-radiation phase-contrast micro computed tomography. *Tissue Eng. Part C Methods* **15**, 403–411. https://doi.org/10.1089/ten.tec.2008.0270.

Bahr, G.F. (1954) Osmium tetroxide and ruthenium tetroxide and their reactions with biologically important substances: electron stains III. *Exp. Cell Res.* **7**, 457–479. https://doi.org/10.1016/S0014-4827(54)80091-7.

Balint, R., Lowe, T. & Shearer, T. (2000) Optimal contrast agent staining of ligaments and tendons for X-ray computed tomography. *PLOS ONE* **11**, e0153552. https://doi.org/10.1371/journal.pone.0153552.

Baruchel, J. (2000) *X-Ray Tomography in Material Science*. Hermes Science, Paris. ISBN: 978-2-7462-0115-6.

Bech, M., Jensen, T.H., Feidenhans, R., Bunk, O., David, C. & Pfeiffer, F. (2009) Soft-tissue phase-contrast tomography with an x-ray tube source. *Phys. Med. Biol.* **54**, 2747–2753. https://doi.org/10.1088/0031-9155/54/9/010.

Cedola, A., Campi, G., Pelliccia, D., *et al.* (2014) Three dimensional visualization of engineered bone and soft tissue by combined X-ray microdiffraction and phase contrast tomography. *Phys. Med. Biol.* **59**, 189–201. https://doi.org/10.1088/0031-9155/59/1/189.

Collaková, J., Křížová, A., Kollarová, V., Dostál, Z., Slabá, M., Veselý, P. & Chmelík, R. (2015) Coherence-controlled holographic microscopy enabled recognition of necrosis as the mechanism of cancer cells death after exposure to cytopathic turbid emulsion. *J. Biomed. Opt.* **20**, 111213. https://doi.org/10.1117/1.JBO.20.11.111213.

Coupe, P., Yger, P., Prima, S., Hellier, P., Kervrann, C. & Barillot, C. (2008) An optimized blockwise nonlocal means denoising filter for 3D magnetic resonance images. *IEEE Trans. Med. Imaging* **27**, 425–441. https://doi.org/10.1109/TMI.2007.906087.

Ge, J., Guo, L., Wang, S., Zhang, Y., Cai, T., Zhao, R.C. & Wu, Y. (2014) The size of mesenchymal stem cells is a significant cause of vascular obstructions and stroke. *Stem Cell Rev.* **10**, 295–303. https://doi.org/10.1007/s12015-013-9492-x.

Giuliani A., Moroncini, F., Mazzoni, S., *et al.* (2014) Polyglicolic acid-polylactide acid scaffold response to different progenitor cell *in vitro* cultures: A demonstrative and comparative X-ray synchrotron radiation phase-contrast microtomography study. *Tissue Eng. Part C Methods* **20**, 308–316. https://doi.org/10.1089/ten.TEC.2013.0213.

Hayes, T.L., Lindgren, F.T. & Gofman, J.W. (1963) A quantitative determination of the osmium tetroxide-lipoprotein interaction. *J. Cell Biol.* **19**, 251–255. https://doi.org/10.1083/jcb.19.1.251.

Herzog, F., Clift, M.J.D., Piccapietra, F., Behra, R., Schmid, O., Petri-Fink, A. & Rothen-Rutishauser, B. (2013). Exposure of silver-nanoparticles and silver-ions to lung cells in vitro at the air-liquid interface. *Part Fibre Toxicol.* **10**, 1–14. https://doi.org/10.1186/1743-8977-10-11.

Hildore, A., Wojtowicz, A. & Johnson, A.W. (2007) Micro-CT based quantification of non-mineralized tissue on cultured hydroxyapatite scaffolds. *J. Biomed. Mater. Res. Part A* **82A**, 1012–1021. https://doi.org/10.1002/jbm.a.31264.

Hofmann, S., Hagenmüller, H., Koch, A.M., Müller, R., Vunjak-Novakovic, G., Kaplan, D.L., Merkle, H.P. & Meinel, L. (2007) Control of in vitro tissue-engineered bone-like structures using human mesenchymal stem cells and porous silk scaffolds: the origin, evolution, and impact of doi moi. *Biomaterials* **28**, 1152–1162. https://doi.org/10.1016/j.biomaterials.2006.10.019.

Jančář, J., Vojtová, L., Nečas, A., Srnec, R., Urbanová, L. & Crha, M. (2009) Stability of collagen scaffold implants for animals with iatrogenic articular cartilage defects. *Acta Vet. Brno* **78**, 643–648. https://doi.org/10.2754/avb200978040643.

Kaiser, J., Holá, M., Galiová, M., *et al.* (2011) Investigation of the microstructure and mineralogical composition of urinary calculi fragments by synchrotron radiation X-ray microtomography:

a feasibility study. *Urol. Res.* **39**, 259–267. https://doi.org/10.1007/s00240-010-0343-9.

Kalasová, D., Zikmund, T. & Kaiser, J. (2016) Phase contrast tomographic imaging of polymer composites. *Materials Structure in Chemistry, Biology, Physics and Technology. Materials Structure*, Vol. **23**, pp. 304–305. Czech and Slovak Crystallographic Association, Czech Republic. ISSN: 1211–5894. http://www.xray.cz/ms/

Kampschulte, M., Langheinirch, A.C., Sender, J., *et al.* (2016). Nano-computed tomography: technique and applications. *Fortschr Röntgenstr*, **188**, 146–154. https://doi.org/10.1055/s-0041-106541.

Khoury, B.M., Bigelow, E.M., Smith, L.M., Schlecht, S.H., Scheller, E.L., Andarawis-Puri, N. & Jepsen, K.J. (2015) The use of nano-computed tomography to enhance musculoskeletal research. *Connect Tissue Res.* **56**, 106–119. https://doi.org/10.3109/03008207.2015.1005211.

Kollarová, V., Collaková, J., Dostál, Z., Veselý, P. & Chmelík, R. (2015) Quantitative phase imaging through scattering media by means of coherence-controlled holographic microscope. *J. Biomed. Opt.* **20**, 111206. https://doi.org/10.1117/1.JBO.20.11.111206.

Komlev, V.S., Mastrogiacomo, M., Peyrin, F., Cancedda, R. & Rustichelli, F. (2009) X-ray synchrotron radiation pseudo-holotomography as a new imaging technique to investigate angio- and microvasculogenesis with no usage of contrast agents. *Tissue Eng. Part C Methods* **15**, 425–430. https://doi.org/10.1089/ten.tec.2008.0428.

Larabell, C.A. & Legros, M.A. (2004) X-ray tomography generates 3D reconstructions of the yeast, Saccharomyces cerevisiae, at 60-nm resolution. *Mol. Biol. Cell* **15**, 957–962. https://doi.org/10.1091/mbc.E03-07-0522.

Le Gros, M.A., Mcdermott, G. & Larabell, C.A. (2005) X-ray tomography of whole cells. *Curr. Opin. Struct. Biol.* **15**, 593–600. https://doi.org/10.1016/j.sbi.2005.08.008.

Lubberts, G. & Rossmann, K. (1967) Modulation transfer function associated with geometrical unsharpness in medical radiography. *Phys. Med. Biol.* **12**, 65–77. https://doi.org/10.1088/0031-9155/12/1/307.

Mather, M.L., Morgan, S.P., White, L.J., Tai, H., Kockenberger, W., Howdle, S.M., Shakesheff, K.M. & Crowe, J.A. (2008). Image-based characterization of foamed polymeric tissue scaffolds. *Biomed. Mater.* **3**, 015011. https://doi.org/10.1088/1748-6041/3/1/015011.

Metscher, B.D. (2009) MicroCT for comparative morphology: simple staining methods allow high-contrast 3D imaging of diverse non-mineralized animal tissues. *BMC Physiol.* **9**, 11–25. https://doi.org/10.1186/1472-6793-9-11.

Momose, A., Takeda, T., Itai, Y. & Hirano, K. (1996) Phase–contrast X–ray computed tomography for observing biological soft tissues. *Nat. Med.* **2**, 473–475. https://doi.org/10.1038/nm0496-473.

Moore, M.J., Jabbari, E., Ritman, E.L., Lu, L., Currier, B.L., Windebank, A.J. & Yaszemski, M.J. (2004) Quantitative analysis of interconnectivity of porous biodegradable scaffolds with micro-computed tomography. *J. Biomed. Mater. Res. A* **71A**, 258–267. https://doi.org/10.1002/jbm.a.30138.

Nečas, A., Plánka, L., Srnec, R., *et al.* (2010) Quality of newly formed cartilaginous tissue in defects of articular surface after transplantation of mesenchymal stem cells in a composite scaffold based on collagen I with chitosan micro- and nanofibers. *Physiol. Res.* **59**, 605–614. ISSN: 1802–9973.

Oliveira, A.L., Malafaya, P.B., Costa, S.A., Sousa, R.A. & Reis, R.L. (2007) Micro-computed tomography (μ-CT) as a potential tool to assess the effect of dynamic coating routes on the formation of biomimetic apatite layers on 3D-plotted biodegradable polymeric scaffolds. *J. Mater. Sci. Mater. Med.* **18**, 211–223. https://doi.org/10.1007/s10856-006-0683-8.

Oliveira, S.M., Ringshia, R.A., Legeros, R.Z., Clark, E., Yost, M.J., Terracio, L., & Teixeira, C.C. (2010) An improved collagen scaffold for skeletal regeneration. *J. Biomed. Mater. Res. A* **94A**, 371–379. https://doi.org/10.1002/jbm.a.32694.

Paganin, D., Mayo, S.C., Gureyev, T.E. Miller P.R. & Willkins, S.W. (2002) Simultaneous phase and amplitude extraction from a single defocused image of a homogeneous object. *J. Microsc.* **206**, 33–40. https://doi.org/10.1046/j.1365-2818.2002.01010.x. ISSN 0022–2720.

Palade, G.E. (1952) A study of fixation for electron microscopy. *J. Exp. Med.* **95**, 285–298. https://doi.org/10.1084/jem.95.3.285.

Palenstijn, W.J., Batenburg, K.J. & Sijbers, J. (2011) Performance improvements for iterative electron tomography reconstruction using graphics processing units (GPUs). *J. Struct. Biol.* **176**, 250–253. https://doi.org/10.1016/j.jsb.2011.07.017.

Papantoniou, I., Sonnaert, M., Geris, L., Luyten, F.P., Schrooten, J. & Kerckhofs, G. (2014) Three-dimensional characterization of tissue-engineered constructs by contrast-enhanced nanofocus computed tomography. *Tissue Eng. Part C Methods* **20**, 177–187. https://doi.org/10.1089/ten.tec.2013.0041.

Prosecká, E., Rampichová, M., Litvinec, A., *et al.* (2015) Collagen/hydroxyapatite scaffold enriched with polycaprolactone nanofibers, thrombocyte-rich solution and mesenchymal stem cells promotes regeneration in large bone defect in vivo. *J. Biomed. Mater. Res. A* **103**, 671–682. https://doi.org/10.1002/jbm.a.35216.

Prosecká, E., Rampichová, M., Vojtová, L., *et al.* (2011) Optimized conditions for mesenchymal stem cells to differentiate into osteoblasts on a collagen/hydroxyapatite matrix. *J. Biomed. Mater. Res.* **99**, 307–315. https://doi.org/10.1002/jbm.a.33189.

Rasband, W.S. (1997–2017) *ImageJ, U. S. National Institutes of Health*. Bethesda, Maryland, USA, http://imagej.nih.gov/ij/.

Riemersma, J.C. (1968) Osmium tetroxide fixation of lipids for electron microscopy. A possible reaction mechanism. *Biochem. Biophys. Acta* **152**, 718–727. https://doi.org/10.1016/0005-2760(68)90118-5.

Scheller, E.L., Troiano, N., Vanhoutan, J.N., *et al.* (2014) Use of osmium tetroxide staining with microcomputerized tomography to visualize and quantify bone marrow adipose tissue *in vivo*. *Methods in Enzymology* (ed. by A. Ormond Macdougald), Vol. **537**, pp. 123–139. Academic Press, Elsevier. ISSN 0076–6879; ISBN 9780124116191.

Schneider, G., Anderson, E., Vogt, S., Knöchel, C., Weiss, D., Legros, M., & Larabell, C. (2002) Computed tomography of cryogenic cells. *Surf. Rev. Lett.* **9**, 177–183. https://doi.org/10.1142/S0218625X02001914.

Sloviková, A., Vojtová, L. & Jančář, J. (2008) Preparation and modification of collagen-based porous scaffold for tissue engineering. *Chem. Pap.* **62**, 417–422. ISSN: 0366–6352.

Starborg, T., Kalson, N.S., Lu, Y., Mironov, A., Cootes, T.F., Holmes, D.F. & Kadler, K.E. (2013) Using transmission electron microscopy and 3View to determine collagen fibril size and three-dimensional organization. *Nat. Protoc.* **8**, 433–448. https://doi.org/10.1038/nprot.2013.086.

Sun, S., Yao, Y., Zou, X., *et al.* (2014) Nano-scale spatial assessment of calcium distribution in coccolithophores using synchrotron-based nano-CT and STXM-NEXAFS. *Int. J. Mol. Sci.* **15**, 23604–23615. https://doi.org/10.3390/ijms151223604.

Taboas, J.M., Maddox, R.D., Krebsbach, P.H. & Hollister, S.J. (2003) Indirect solid free form fabrication of local and global porous, biomimetic

and composite 3D polymer-ceramic scaffolds. *Biomaterials* **24**, 181–194. https://doi.org/10.1016/S0142-9612(02)00276-4.

Tesařová, M., Zikmund, T., Kaucká, M., Adameyko, I., Jaroš, J., Paloušek, D., Škaroupka, D. & Kaiser, J. (2016) Use of micro computed-tomography and 3D printing for reverse engineering of mouse embryo nasal capsule. *J. Instrum.* **11**, C03006. https://doi.org/10.1088/1748-0221/11/03/C03006.

Van Aarle, W., Palenstijn, W.J., Cant, J., *et al.* (2016) Fast and flexible X-ray tomography using the ASTRA toolbox. *Opt. Express* **24**, 25129–25147. https://doi.org/10.1364/OE.24.025129.

Van Aarle, W., Palenstijn, W.J., De Beenhouwer, J., Altantzis, T.A., Bals, S., Batenburg, K.J. & Sijbers, J. (2015) The ASTRA Toolbox: a platform for advanced algorithm development in electron tomography. *Ultramicroscopy* **157**, 35–47. https://doi.org/10.1016/j.ultramic.2015.05.002.

Van der Rest, M. & Garrone, R. (1991) Collagen family of proteins. *FASEB J.* **5**, 2814–2823.

Weitkamp, T., Haas, D., Wegrzynek, D. & Rack, A. (2011) ANKAphase: software for single-distance phase retrieval from inline X-ray phase-contrast radiographs. *J. Synchrotron Radiat.* **18**, 617–629. https://doi.org/10.1107/S0909049511002895.

Wu, X. & Liu, H. (2007) Clarification of aspects in in-line phase sensitive X-ray imaging. *Med. Phys.* **34**, 737–743. https://doi.org/10.1118/1.2431475.

Yang, Y., Dorsey, S.M., Becker, M.L., Lin-Gibson, S., Schumacher, G.E., Flaim, G.M., Kohn, J. & Simon, C.G.J. (2008) X-ray imaging optimization of 3D tissue engineering scaffolds via combinatorial fabrication methods. *Biomaterials* **29**, 1901–1911. https://doi.org/10.1016/j.biomaterials.2007.12.042.

Žídek, J., Vojtová, L., Abdel-Mohsen, A.M., *et al.* (2016) Accurate micro-computed tomography imaging of pore spaces in collagen-based scaffold. *J. Mater. Sci. Mater. Med.* **27**, 1–18. https://doi.org/10.1007/s10856-016-5717-2.

Supporting Information

Additional supporting information may be found online in the Supporting Information section at the end of the article.

Supplementary material S1: (A) Detail of SEM image of MSC adhering on collagen fibre in scaffold (B) EDX mapping analysis of osmium (green colour) and carbon (red colour) in the surface of the sample. Osmium has origin from the contrast agent and carbon comes from the collagen scaffold.

Supplementary material S2: A part of CT slice of collagen porous scaffold seeded with MSCs, (A) original data (B) after filtration and application of phase retrieval algorithm.